

PAPER • OPEN ACCESS

## Electron correlation dynamics in atomic Kr excited by XUV pulses and controlled by NIR laser pulses of variable intensity

To cite this article: Andreas H Roos *et al* 2023 *New J. Phys.* **25** 013038

View the [article online](#) for updates and enhancements.

You may also like

- [Attosecond transient absorption of argon atoms in the vacuum ultraviolet region: line energy shifts versus coherent population transfer](#)  
Wei Cao, Erika R Warrick, Daniel M Neumark *et al.*
- [Ultrafast dynamics of adenine following XUV ionization](#)  
Erik P Månsson, Simone Latini, Fabio Covito *et al.*
- [Collinear dual-pulse laser optical breakdown and energy deposition](#)  
Andrea Alberti, Alessandro Munafó, Carlos Pantano *et al.*



## PAPER

## Electron correlation dynamics in atomic Kr excited by XUV pulses and controlled by NIR laser pulses of variable intensity

## OPEN ACCESS

## RECEIVED

20 October 2022

## REVISED

11 January 2023

## ACCEPTED FOR PUBLICATION

23 January 2023






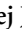







## PUBLISHED

2 February 2023

Original Content from  
this work may be used  
under the terms of the  
[Creative Commons  
Attribution 4.0 licence](https://creativecommons.org/licenses/by/4.0/).

Any further distribution  
of this work must  
maintain attribution to  
the author(s) and the title  
of the work, journal  
citation and DOI.



Andreas H Roos<sup>1,\*</sup> , Ziaul Hoque<sup>1</sup> , Eva Klimešová<sup>1</sup> , Ltaief Ben Ltaief<sup>2</sup> , Cristian Medina<sup>3</sup> ,  
Matej Jurkovič<sup>1,4</sup> , Martin Albrecht<sup>1,4</sup> , Ondřej Finke<sup>1,4</sup> , Ondřej Hort<sup>1</sup> ,  
Jaroslav Nejd<sup>1,4</sup> , Marcel Mudrich<sup>2</sup> , Jakob Andreasson<sup>1</sup>  and Maria Krikunova<sup>1,5</sup> 

<sup>1</sup> ELI Beamlines Facility, The Extreme Light Infrastructure ERIC, Za Radnicí 835, Dolní Břežany, 252 41, Czech Republic

<sup>2</sup> Department of Physics and Astronomy, Aarhus University, 8000 Aarhus C, Denmark

<sup>3</sup> Physikalisches Institut, Universität Freiburg, 79104 Freiburg, Germany

<sup>4</sup> Czech Technical University in Prague, FNSPE, Břehová 7, Prague, 11519, Czech Republic

<sup>5</sup> Wildau Technical University of Applied Sciences, Hochschulring 1, 15745 Wildau, Germany

\* Author to whom any correspondence should be addressed.

E-mail: [andreas.roos@eli-beams.eu](mailto:andreas.roos@eli-beams.eu)

**Keywords:** electron correlation, control ionization dynamics, krypton satellite states, XUV/NIR pump-probe, HHG, quantum beating oscillation, doubly excited states

## Abstract

We have investigated the possibility to track and control correlation dynamics of valence electrons in krypton (Kr) initiated by the absorption of one extreme ultraviolet (XUV) photon. In this investigation, pump-probe experiments have been performed where monochromatized single high-harmonics at photon energies 29.6, 32.8, and 35.9 eV have been used as pump to populate different intermediate excited states. A temporally delayed near-infrared (NIR) pulse probes the population of various decay channels via the detection of Kr<sup>2+</sup> ion yields and its transient profiles. We observe that by varying the NIR pulse intensity within a range from  $0.3 \times 10^{13}$  to  $2.6 \times 10^{13}$  W cm<sup>-2</sup>, the shape of the Kr<sup>2+</sup> transient profile changes significantly. We show that by varying the intensity of the NIR pulse, it is possible—(i) to control the ratio between sequential and non-sequential double ionization of Kr; (ii) to selectively probe quantum beating oscillations between Kr<sup>+\*</sup> satellite states that are coherently excited within the bandwidth of the XUV pulse; and (iii) to specifically probe the relaxation dynamics of doubly excited (Kr<sup>\*\*</sup>) decay channels. Our studies show that the contribution of different ionization and decay channels (i)–(iii) can be altered by the NIR pulse intensity, thus demonstrating an efficient way to control the ionization dynamics in rare gas atoms.

## 1. Introduction

Photoelectron spectroscopy with ultra-short femto- to attosecond pulses has been developed into a powerful technique to capture ultrafast electron dynamics in atoms, molecules, nano-particles and solids [1–5]. In recent applications, fundamental questions such as the delay in photoemission from atoms to solids [3], electron correlations in multi-electron systems [3, 4], complex photoinduced dynamics in molecules [3, 4, 6], and nano-particles [7–9] have been addressed.

Time-resolved photoelectron spectroscopy directly benefits from the sensitivity of kinetic energies of emitted electrons to the specific electronic configuration of the sample. To understand experimental time-resolved spectra, high-resolution steady-state electron spectra as well as support from theory are instrumental. Main experimental challenges limiting high spectral resolution in electron spectroscopy are the broad spectral bandwidth of ultrashort extreme ultraviolet (XUV) pulses, possible space-charge effects and significant background signal often produced by strong laser fields or secondary electrons [10, 11].

Compared to electron spectroscopy, ion detection schemes are in many cases more robust and straightforward. Indeed, ion charge states populated by a combined action of XUV and optical laser fields are

usually less affected by background. Moreover, ions are less sensitive to distortions caused by e.g. electric and magnetic fields in the interaction region. Selected examples of phenomena probed by ion charge state spectroscopy on atoms are observation of strong-field induced tunnel ionization [12], time-domain observation of the dynamics of Auger decay [12–14], study of Rabi oscillations, excited by the resonant coupling of ionic ground to ionic excited states [15], as well as determination of lifetimes and cross-sections of atomic excited states, populated by the absorption of XUV photons [16, 17]. Additionally, ion spectroscopy has developed into a practical and very robust diagnostic technique to determine time-zero and temporal resolution in XUV and near-infrared (NIR) pump-probe experiments [13].

The number of available decay channels accessible upon one-photon absorption in atoms may be huge [18]. Therefore, the lack of sensitivity of ion spectroscopy to specific electronic configurations is commonly considered as a main disadvantage of this detection scheme. One strategy to obtain better spectral selectivity in ion spectroscopy was demonstrated recently [10]. By tuning the intensity of the probing NIR laser field, it is possible to specifically select different groups of Auger decay channels, thus providing efficient control of the dynamics of intermediate excited states in atomic krypton.

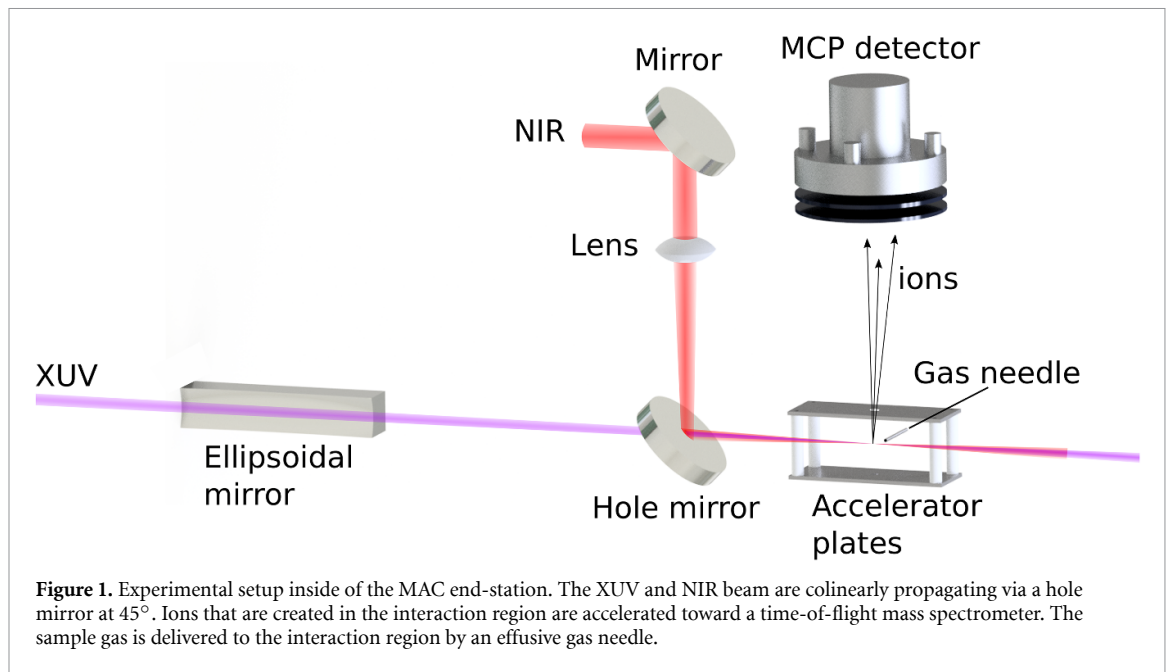
In the current study, we further investigate the possibility to control the dynamics of the available ionization and decay channels following the absorption of one XUV photon in Kr atoms. We use high-order harmonics (HH) 19, 21 and 23 to initiate excited state dynamics in Kr. Available steady-state spectroscopy data and theoretical calculations allows us to identify intermediate excited states while using selected harmonics. The synchronized NIR pulse then probes the population of various possible decay channels as the intensity of the NIR pulse is varied within the range from  $0.3 \times 10^{13}$  to  $2.6 \times 10^{13}$  W cm<sup>-2</sup>. We observe that by tuning the intensity of the NIR probe pulse, different pathways caused by electron correlation dynamics become visible in the measurement of the transient Kr<sup>2+</sup> ion yield.

## 2. Experimental method

The experiment has been performed at the MAC end-station [19], at ELI Beamlines, located at the end of a HHG beamline [20]. The Ti:Sapphire drive laser of the HHG beamline (Legend Elite Duo from Coherent) operates at a repetition rate of 1 kHz with a central wavelength at 792 nm and the pulse duration of  $\sim 30$  fs. The drive laser has a pulse energy of about 12 mJ, and is passed through a 90:10 beamsplitter where the reflected 90% drives the HHG beamline and transmitted 10% of the NIR pulse is directed out of vacuum and coupled into the MAC chamber via a delay line. The HH are generated by focusing the NIR beam with a spherical mirror of 5 m focal length into a Kr filled gas cell. For the time resolved measurements, the relative delay between the XUV-pump and NIR-probe pulse was controlled by the delay line with a total travel range of 1 m (6 ns), with a minimum temporal delay step of  $< 3$  fs.

A time-preserving grating monochromator [21, 22] located further down the HHG beamline selects a single harmonic with a 200  $\mu\text{m}$  slit. Residual NIR is filtered by a 200 nm thick Al-foil placed before the monochromator. The photon flux in each harmonic was measured by an intensity-calibrated XUV photodiode in the MAC vacuum chamber, and is  $1 \times 10^7$  photons/shot for HH19,  $6 \times 10^6$  photons/shot for HH21, and  $2 \times 10^6$  photons/shot for HH23. The FWHM energy bandwidth for the harmonics is about 300 meV as measured by a flat-field XUV spectrometer located after the monochromator.

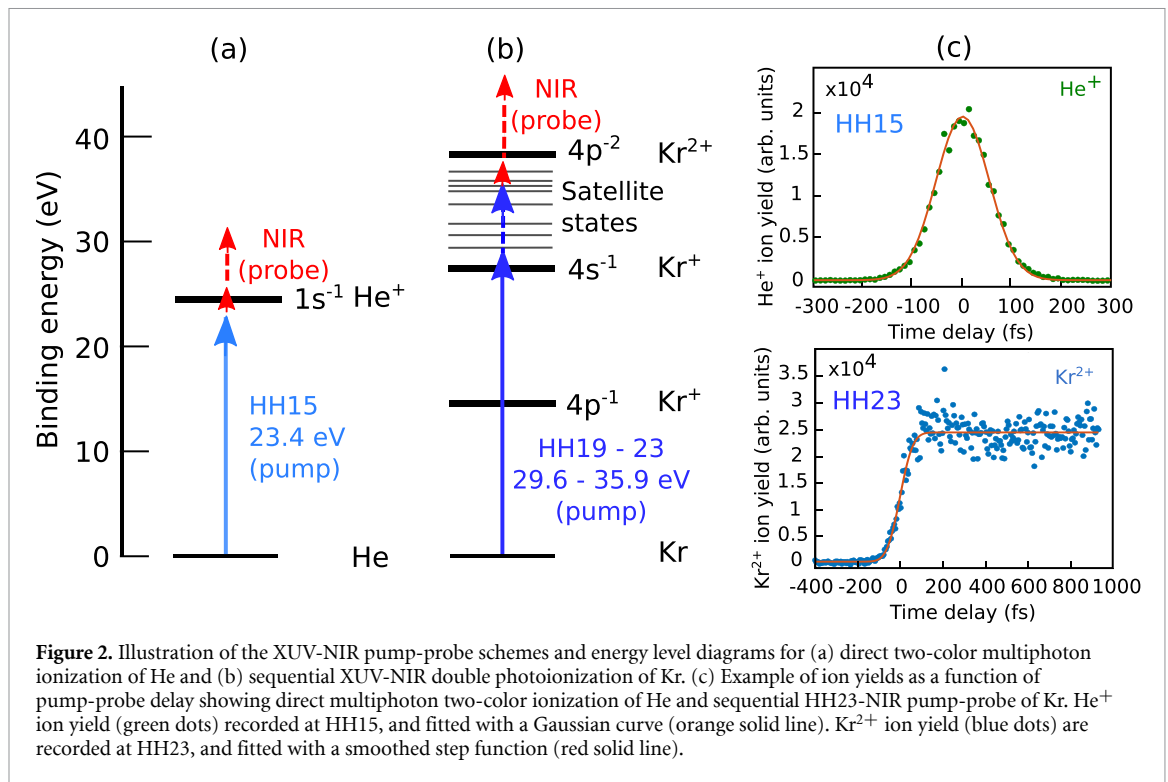
The XUV and NIR beams are focused colinearly into the interaction region according to the experimental setup displayed in figure 1. The XUV beam is focused by an ellipsoidal mirror with 500 mm focal length, and the NIR beam is focused by a lens of 200 mm focal length. The Kr sample gas ( $> 99.99\%$  purity) is delivered into the interaction region by an effusive capillary placed a few millimeters from the focus of the two beams. Ions created in the interaction region are accelerated by an electric field of  $100 \text{ V mm}^{-1}$  between two accelerator plates, and detected by a microchannel plate (MCP) detector (Hamamatsu F9892-31) placed  $\sim 200$  mm from the interaction region. The spatial overlap of the XUV and NIR beams is ensured by an imaging line using a Ce:YAG fluorescence screen in the focal plane. The XUV and NIR focal spot diameters are about  $30 \times 40 \mu\text{m}^2$  and  $15 \times 30 \mu\text{m}^2$ , respectively. The pulse duration of the XUV pulse is comparable to the driving NIR pulse, and is  $< 50$  fs. The probe NIR pulses experience temporal broadening while propagating through optical elements and in air, and its temporal width inside the experimental chamber is measured to be  $\sim 150$  fs from FROG measurements. The NIR-probe beam is attenuated by neutral density filters placed in front of the experimental end-station. The uncertainty in the estimation of the NIR intensities is about 25%, based on the combined uncertainty from the power meter, Gaussian focus spot size diameter ( $1/e^2$ ), and estimated losses on optical surfaces.



### 3. Results and discussion

Our present time-dependent investigation of the  $\text{Kr}^+$  satellite states is made using HH19 (29.6 eV), HH21 (32.8 eV), and HH23 (35.9 eV) as the XUV-pump, and a NIR probe (1.56 eV) in a range of intensities between  $0.3 \times 10^{13}$  to  $2.6 \times 10^{13} \text{ W cm}^{-2}$ . In this NIR intensity range only a small amount of  $\text{Kr}^+$  in the lowest lying electronic states can be produced [17], which is also confirmed in our  $\text{Kr}^{2+}$  ion yield measurements. At intensities up to about  $2 \times 10^{13} \text{ W cm}^{-2}$ , direct double ionization is about seven orders of magnitude lower than single ionization with the NIR alone [17]. Therefore, the path to generate a significant amount of  $\text{Kr}^{2+}$  is through XUV photo-ionization and -excitation of the Kr to satellite states above the  $4 s^{-1}$  threshold, which are then further ionized by multi-photon NIR absorption. The intermediate  $\text{Kr}^{+*}$  satellite states populated by the XUV pulse are relatively long-lived ( $\gg 1$  ps), therefore the transient profile of the  $\text{Kr}^{2+}$  signal can be approximated by a smoothed step function [13]. At  $2.6 \times 10^{13} \text{ W cm}^{-2}$  a noticeable amount of singly ionized Kr is produced by the NIR pulse alone, which can be seen from a non-zero offset of the ion yield at negative time delays (see figure 3(d)). The photoionization processes of atomic Kr by HH19, HH21, and HH23 leading to the population of the satellite states have partial cross sections about 2 to 3 orders of magnitude higher compared to the photoionization leading to the  $4p^6 4 s^{-1} {}^2S_{1/2}$  final state [17]. Therefore, it can be assumed that the dominant contribution to the  $\text{Kr}^{2+}$  ion yield signal comes from multi-photon ionization of satellite states.

The time-dependent ion yield for  $\text{Kr}^{2+}$  as a function of the HH23-pump NIR-probe time delay, is shown in figure 2(c). The ion yields are obtained from the integrated ion spectra from 3000 laser pulses at each delay position. The time resolution and maximum time overlap between the XUV and NIR pulses were determined from the HH15-NIR pump-probe ion yield signal obtained from helium (He) atoms (figure 2(c)). To reach the single ionization threshold for He, the combined energy from one HH15 (23.4 eV) photon and one NIR (1.56 eV) photon is required, as seen from the energy level diagram in figure 2(a). The profile of the transient signal may then be described as a Gaussian convolution of the XUV and NIR pulses, with the maximum overlap of the beams representing time zero, as seen in figure 2(c). The time zero for all other measurements in this study is therefore taken as relative to the delay line position obtained from He HH15-NIR pump-probe measurements. The  $\text{Kr}^{2+}$  ion yields obtained with HH23 follows a step-like transient profile as a function of the pump-probe time delay, which is in good agreement with the work reported in [17]. The step in ion yield is characteristic of sequential two-color double ionization via long-lived ( $\gg$ ps)  $\text{Kr}^{+*}$  satellite states, as illustrated in figure 2(b). The satellite states involved in this process have been identified by earlier studies [23–26], and are populated by either the process of shake-up following 4p photoionization or configuration interaction (CI) following 4s photoionization. Aside from sequential double photoionization, no other pathways leading to doubly ionized Kr may be discerned from the time dependent ion yields recorded at NIR intensities between  $0.3 \times 10^{13}$  to  $2.6 \times 10^{13} \text{ W cm}^{-2}$ , as previously reported in [17].

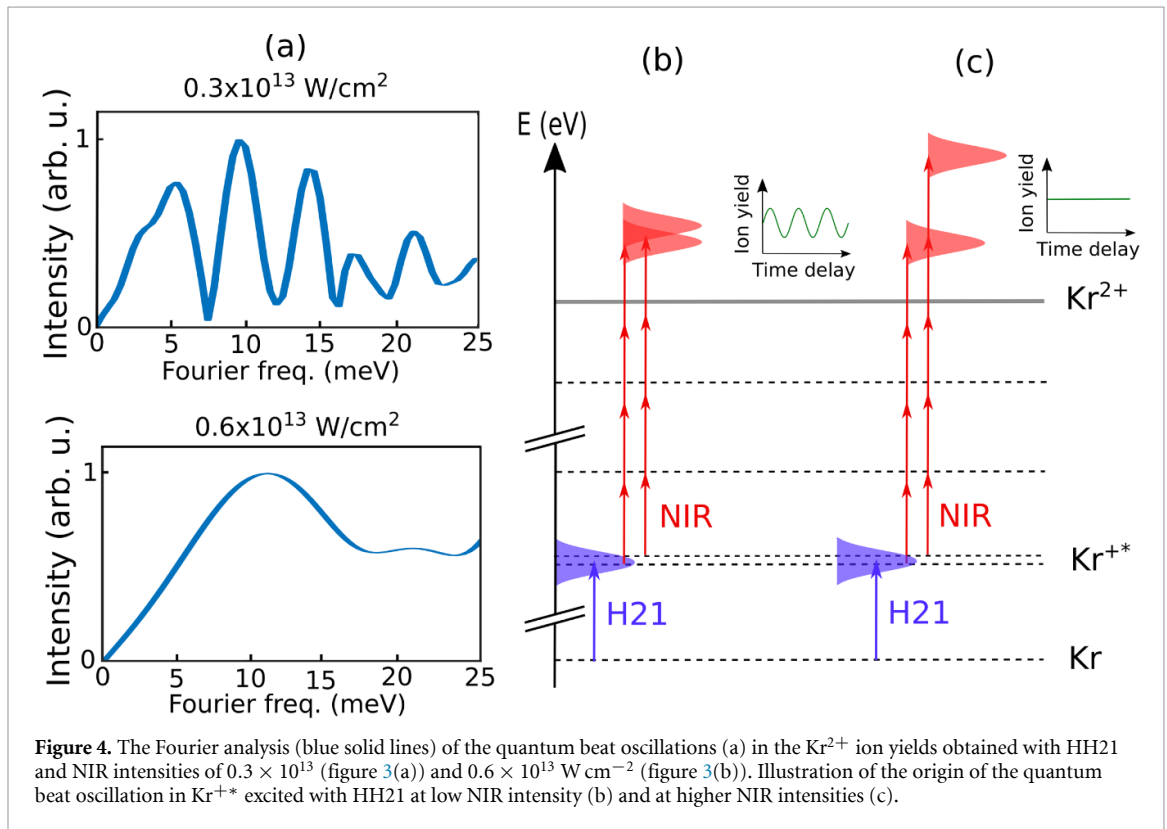
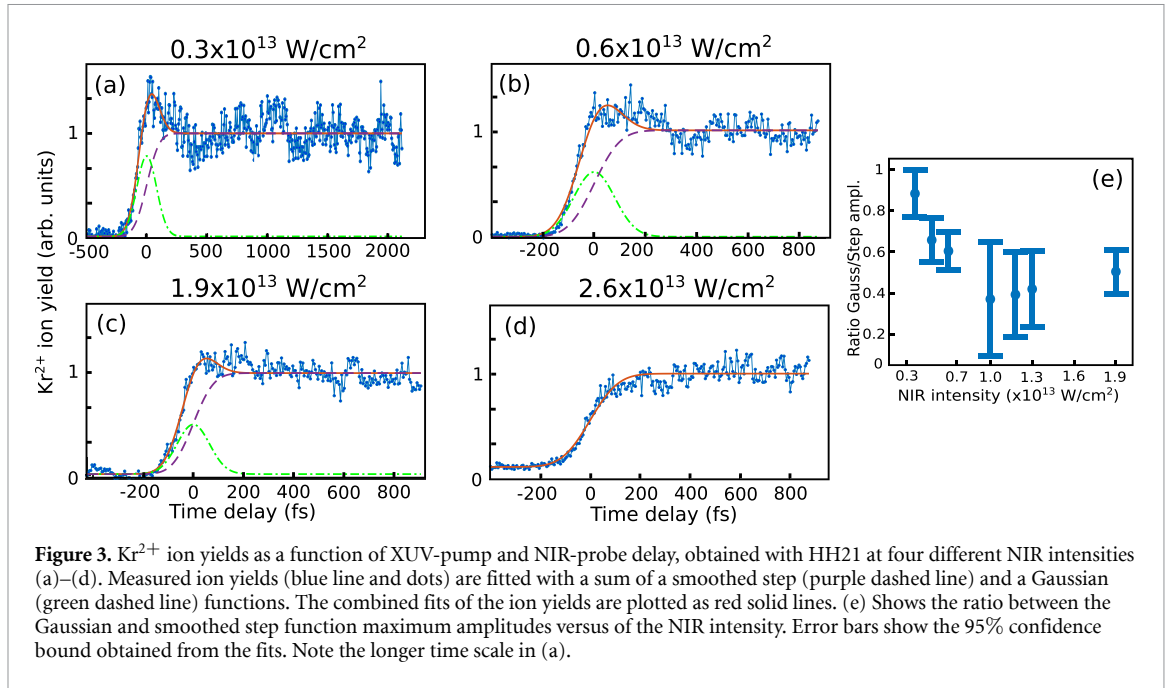


### 3.1. Electron correlation dynamics initiated by HH21

Measurements of the time-dependent Kr<sup>2+</sup> ion yield with HH21 as pump pulse can be seen in figure 3. Compared to the corresponding measurements with HH23, the Kr<sup>2+</sup> ion yields obtained with HH21 shows more structure. In addition to the step-like behavior, there is an enhancement of the yield starting from zero time delay, which we attribute to simultaneous non-sequential two-color multi-photon double ionization. In figure 3, the ion yields have been fitted by sums of smoothed step and Gaussian functions, representing the sequential and non-sequential pathway contributions, respectively. A clear gradual change of the shape of the ion yield curves can be seen as the NIR intensity is increased from  $0.3 \times 10^{13}$  to  $2.6 \times 10^{13}$  W cm<sup>-2</sup>. The direct two-color multi-photon double ionization is more pronounced at lower NIR intensities, and not discernible at an intensity of  $2.6 \times 10^{13}$  W cm<sup>-2</sup>. The relatively lower signal from the non-sequential path may be attributed to an increase in tunnel ionization from the populated satellite states in Kr<sup>+</sup> with increasing NIR intensity. Our finding is supported by the study of multi-photon double ionization in helium in one-color NIR-field [27], where the non-sequential multi-photon ionization is dominant at low NIR-field strength and the sequential mechanisms contributes more with increasing NIR-field strength. The case for XUV-NIR two-color non-sequential double ionization in helium has been investigated in [28]. According to [28], the XUV laser field mainly determines the probability of the double ionization and the NIR mainly contributes to the line width in the above threshold ionization (ATI) spectrum, which is in line with the relatively lower contribution of non-sequential double ionization at higher NIR intensity in figure 3.

The ratio between the Gaussian and smoothed step function amplitudes versus the NIR intensity is shown in figure 3(e). This plot gives an estimate of the amount of sequential double ionization that goes through long-lived satellite states relative to the amount of non-sequential pathways as a function of the NIR intensity. The earlier study in [17] did not report the appearance of non-sequential ionization in the Kr<sup>2+</sup> ion yield, which may be explained by the relatively high NIR intensity ( $2 \times 10^{13}$  W cm<sup>-2</sup>) used. Indeed, the transient profile of Kr<sup>2+</sup> ion yields obtained above  $2 \times 10^{13}$  W cm<sup>-2</sup> (see figure 3(d)) in our study is similar to the previously reported measurement with HH21. The ion yield in figure 3(d) is dominated by the signal from the sequential pathways, therefore the data point at  $2 \times 10^{13}$  W cm<sup>-2</sup> is not included in figure 3(e). An estimated upper limit to the ratio between the Gaussian and step function amplitudes is  $<0.3$ . Below this limit the shape of the transient profile is dominated by the step function.

In addition to the sequential and non-sequential contributions to the Kr<sup>2+</sup> transient ion yield, an oscillatory feature is resolved with HH21 at NIR intensities below  $0.9 \times 10^{13}$  W cm<sup>-2</sup> (figures 3(a) and (b)). The oscillations arise from quantum beating of interfering neighboring satellite states, which has previously been experimentally and theoretically investigated in depth for the case of Ne [29]. The quantum beating is the result of photoionization of bound time-dependent electron wave packets by a short laser pulse, as



visualized in figures 4(b) and (c). The XUV (HH21) pulse may photo-ionize and -excite the Kr atoms to a coherent superposition of satellite states, which may be further photoionized by the NIR pulse. The quantum beating arises from the interference of the ionization pathways leading to the same final state in the continuum. The beating period of the ion yield reflects the energy difference between the involved states, and may be used for time-dependent tracing of Rydberg electrons [30] and spin precession in coherently excited states [31]. In order to quantify the oscillations in the ion yields, Fourier transformation was performed using the limits of the delay scan from 0 fs up to the end of the scan. The quantum beating in the  $\text{Kr}^{2+}$  ion yield obtained at NIR intensities of  $0.3 \times 10^{13}$  and  $0.6 \times 10^{13} \text{ W cm}^{-2}$  is shown in figure 4(a). The limits for the time integration gives a corresponding maximum energy resolution in the Fourier frequency of about 2 and 5 meV for the ion yields obtained at  $0.3 \times 10^{13}$  and  $0.6 \times 10^{13} \text{ W cm}^{-2}$ , respectively. The Fourier analysis for

**Table 1.** Possible states involved in the quantum beat oscillations in the  $\text{Kr}^{2+}$  ion yield obtained with HH21 (32.8 eV).

Numbers <sup>a</sup>	State assignments <sup>b</sup>	$\Delta E^c$ (meV)
11–12	$(^1\text{D})5s\ ^2\text{D}_{5/2} - (^3\text{P})4d\ ^4\text{F}_{7/2}$	8
13–14	$(^3\text{P})4d\ ^4\text{P}_{1/2} - (^3\text{P})4d\ ^4\text{F}_{5/2}$	22
27–28	Unknown–unknown	12
28–29	Unknown– $(^3\text{P})5p\ ^2\text{P}_{1/2}$	16
35–36	Unknown– $(^1\text{S})5s\ ^2\text{S}_{1/2}$	20
38–39	$(^1\text{D})4d\ ^2\text{D}_{5/2} - (^1\text{D})5p\ ^2\text{F}_{7/2}$	23
42–43	$(^1\text{D})4d\ ^2\text{P}_{1/2} + (^1\text{D})5p\ ^2\text{D}_{3/2} - (^1\text{D})5p\ ^2\text{P}_{1/2}$	6
42–44	$(^1\text{D})4d\ ^2\text{P}_{1/2} + (^1\text{D})5p\ ^2\text{D}_{3/2} - (^1\text{D})5p\ ^2\text{D}_{5/2}$	16
43–44	$(^1\text{D})5p\ ^2\text{P}_{1/2} - (^1\text{D})5p\ ^2\text{D}_{5/2}$	10

<sup>a</sup> Numbers according to observed peaks in [25].

<sup>b</sup> State assignment given in table 1 in [25].

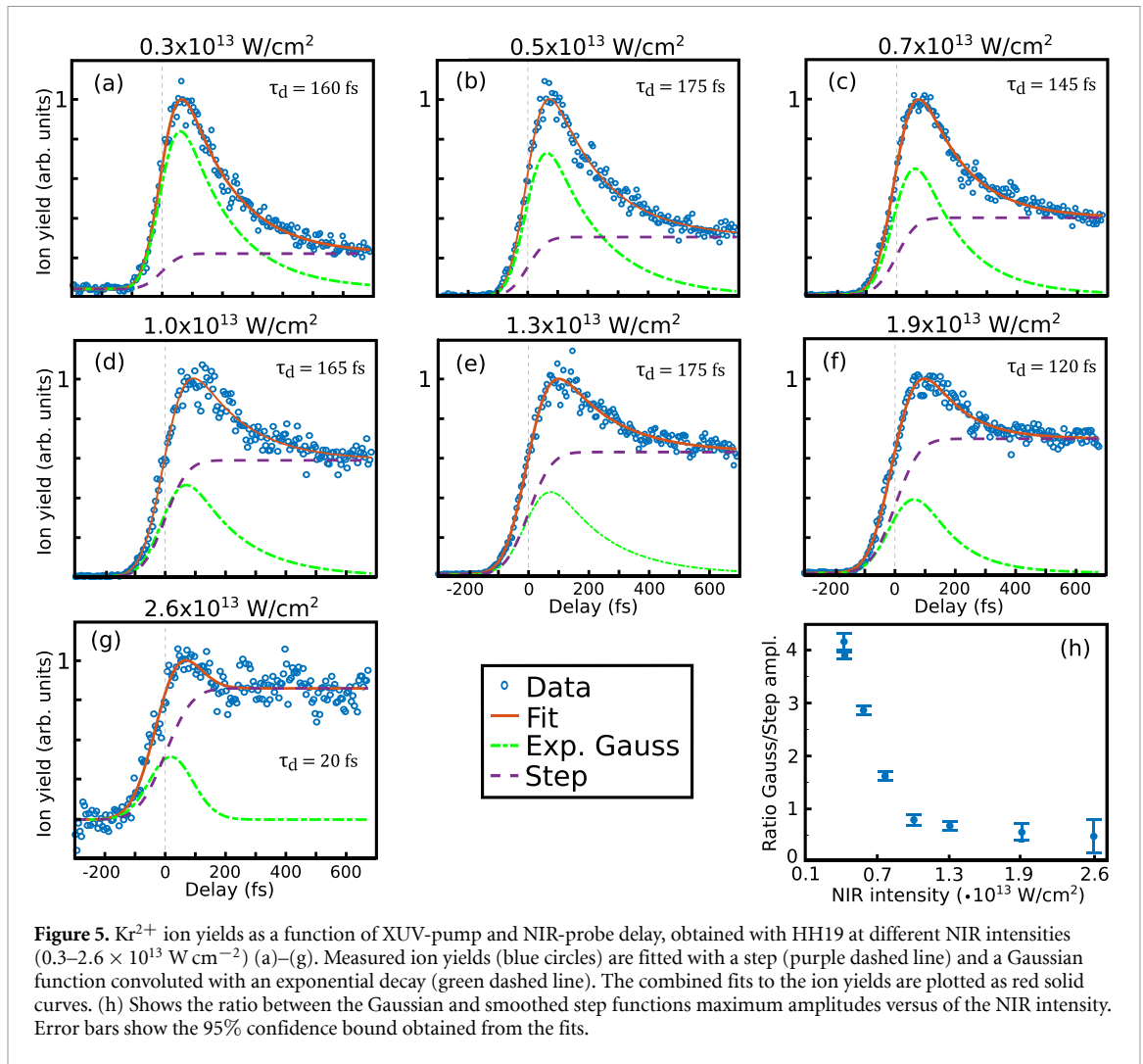
<sup>c</sup> Energy difference between states given in [25].

the ion yield recorded at  $0.3 \times 10^{13} \text{ W cm}^{-2}$  shows several resolved peaks below 25 meV, with the three main peaks at about 5, 10, and 14 meV. State pairs that can be populated by HH21 and that may be the source of the beating can be identified from the works in references [23, 25, 26], and are listed in table 1. The table also contains several state pairs that could be the origin of the weaker quantum beat oscillations obtained between 17 and 25 meV. The Fourier analysis for the ion yield recorded at  $0.6 \times 10^{13} \text{ W cm}^{-2}$  is less resolved, and shows a single broad peak with maximum at about 11 meV. A limiting factor for the observation of quantum beating oscillations above 25 meV is the relatively long temporal width of the NIR pulse of 150 fs ( $\sim 27$  meV).

Note that as the NIR intensity is increased above  $0.6 \times 10^{13} \text{ W cm}^{-2}$ , the beating oscillations are gradually suppressed, and at a NIR intensities above  $1.9 \times 10^{13} \text{ W cm}^{-2}$  no clear beating can be seen in the ion yield signal. In the study of quantum beating in excited Ne by Geiseler *et al* [29], a strong oscillation amplitude that increases with the NIR intensity in the  $0.5\text{--}2.5 \text{ TW cm}^{-2}$  range was observed. This was attributed to the increase of AC Stark shift or stronger coupling to different states with increasing NIR intensity. Indeed, the NIR laser intensity may modify the excited-state wave packet during the ionization while an increasing NIR intensity facilitates AC Stark shifts, which may lead to smaller energy separation between the satellite states [29]. This may in principle induce either an increase or a decrease of the beating amplitudes. In the case considered here we suggest that at a low NIR intensity the dominant ionization pathway to reach  $\text{Kr}^{2+}$  from the satellite states involves the absorption of an exact number of NIR photons to overcome the double ionization energy, as illustrated in figure 4(b). As the intensity increases, the probability to absorb more photons above the double ionization energy also increases, i.e. ATI. The probability of higher order ATI depends strongly on the NIR intensity, which means that a larger number of final electronic states in the continuum may be reached at higher NIR intensities. This is illustrated in figure 4(c). As the intensity increases, multiple pathways that are leading to different final states become possible. Therefore, the interference of the coherently excited wave packets is effectively suppressed at high NIR intensity. We suggest, that due to the relatively high intensity of  $>2 \times 10^{13} \text{ W cm}^{-2}$  quantum- beating oscillations are suppressed by higher order ATI and are therefore not observed in the transient  $\text{Kr}^{2+}$  ion yields, similar to [17]. Also, no quantum beating oscillations can be seen in the ion yields obtained with HH23, which may also be explained by higher order ATI that effectively suppresses quantum interference of final states in the continuum. At HH23, even higher energetic satellite states may be reached, i.e. an even lower NIR intensity is required for the final double ionization process resulting in a much lower NIR intensity required to observe quantum beat oscillations with HH23 as pump compared to HH21.

### 3.2. Electron correlation dynamics initiated by HH19

Measurements of the time-dependent  $\text{Kr}^{2+}$  ion yields with HH19 as pump can be seen in figure 5. Compared to the ion yields recorded with HH21 and HH23, the shape of transient  $\text{Kr}^{2+}$  ion yield recorded with HH19 is highly sensitive to the NIR intensity. At a NIR intensity of  $0.3 \times 10^{13} \text{ W cm}^{-2}$  the ion yield is dominated by an enhanced signal close to zero pump-probe delay, while at higher NIR intensities a gradual enhancement of the ion yield at longer delays is observed. The total  $\text{Kr}^{2+}$  ion yields in figure 5 can be fitted well by the sum of a smoothed step function and a Gaussian function convoluted with an exponential decay. Similar as for the ion yields obtained with HH21 and HH23, the smoothed step function originates from the sequential double photoionization pathways involving the long-lived satellite states above the  $4\text{ s}^{-1} \ ^2\text{S}_{1/2}$  threshold ( $\sim 27.5$  eV). The satellite states that can be reached by HH19 are mainly populated by shake-up following 4p photoionization, with  $(^3\text{P})5\text{ s}$  and  $(^3\text{P})4\text{ d}$  as the leading configurations [17, 24, 25]. Compared to the ion yields obtained with HH21 and HH23, the ones recorded with HH19 have a much smaller relative



**Figure 5.**  $\text{Kr}^{2+}$  ion yields as a function of XUV-pump and NIR-probe delay, obtained with HH19 at different NIR intensities ( $0.3\text{--}2.6 \times 10^{13} \text{ W cm}^{-2}$ ) (a)–(g). Measured ion yields (blue circles) are fitted with a step (purple dashed line) and a Gaussian function convoluted with an exponential decay (green dashed line). The combined fits to the ion yields are plotted as red solid curves. (h) Shows the ratio between the Gaussian and smoothed step functions maximum amplitudes versus of the NIR intensity. Error bars show the 95% confidence bound obtained from the fits.

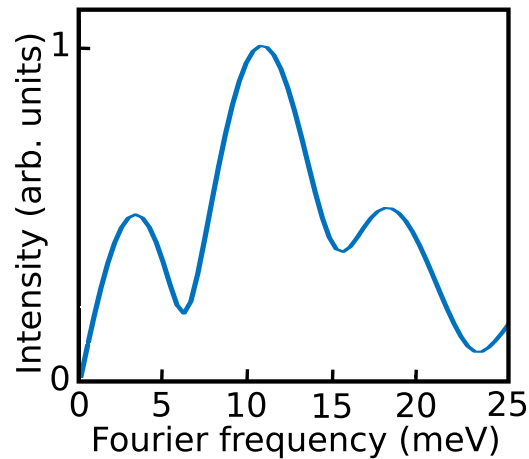
contribution of sequential two-color double photoionization, especially for the yields recorded at the lower NIR intensities. This is explained by the higher binding energy of the states that can be populated by HH19 compared to the binding energy of states that can be populated by the higher harmonics [23–26]. Furthermore, the ion yields in figure 5 reveal fast electron dynamics as represented by the fit of a Gaussian function convoluted with an exponential decay. The ratio between the Gaussian and smoothed step function amplitudes versus the NIR intensity is plotted in figure 5(h). This plot provides an estimate for the relative contribution of sequential double ionization that goes through the long-lived satellite states as a function of the NIR intensity.

The main feature that can be noted from the convoluted Gaussian is the exponential decay  $\tau_d = 160 \pm 25 \text{ fs}$  (figures 5(a)–(f)) of the ion yield signal around zero pump-probe delay. Similar long decay times have previously been observed in inner-shell relaxation dynamics in noble gas atoms [13, 18]. We cannot identify the energetic origin from the ion measurements, which prohibits a further complete assignment. Note that, the presence of multiple close lying short-lived two-electron states within the energy bandwidth of the XUV cannot be resolved in the ion yield under our experimental conditions, but will affect the apparent value of the decay time  $\tau_d$ .

At higher NIR intensity ( $2.6 \times 10^{13} \text{ W cm}^{-2}$ ), the decay time decreases to  $\tau_d = 20 \pm 5 \text{ fs}$ . A reason for why the  $\tau_d$  decay time decreases with increasing NIR intensity is not yet understood. However, within the energy bandwidth of HH19 ( $29.6 \pm 0.15 \text{ eV}$ ) several doubly-excited states ( $\text{Kr}^{**}$ ) may be reached with the ( $^1\text{D}$ ) $4d5p$  main electronic configuration [32, 33], which has much shorter lifetimes compared to the singly ionized satellite states. The lifetimes of the strongest two-electron excited states are about 14, 34, and 19 fs as predicted theoretically in [33] for the state numbers 13, 14, and 15, respectively. We suggest that one possible origin for the short decay time  $\tau_d = 20 \text{ fs}$  recorded at  $2.6 \times 10^{13} \text{ W cm}^{-2}$  NIR intensity may be due to these doubly excited states.

Notably, at a NIR intensity of  $2.6 \times 10^{13} \text{ W cm}^{-2}$ , an oscillatory feature in the ion yield recorded with HH19 emerges (figure 6). The Fourier analysis gives a frequency maximum corresponding to about 11 meV





**Figure 6.** Fourier analysis of the quantum beating in the ion yield observed with HH19 at a NIR intensity of  $2.6 \times 10^{13} \text{ W cm}^{-2}$  (figure 5(g)).

(with 5 meV energy resolution) which is comparable to the most intense oscillations obtained with HH21 (figure 4(a)). Other smaller frequency peaks can be seen at about 4 and 18 meV, which is similar to what is observed in figure 4(a). This similarity may indicate that the same states are involved in the quantum beating. However, no satellite states with the energy separation corresponding to a quantum beating of  $<30 \text{ meV}$  can be directly populated by HH19 alone. A possible explanation to the quantum beating resolved in figure 6 is that the NIR pulse starts to couple satellite states populated by HH19 up to other bound states above 29.6 eV (HH19) which are then photoionized within the same NIR pulse. This scenario is similar to the observation reported in [29].

#### 4. Summary

In conclusion, monochromatic XUV radiation from HHG and high-intensity NIR pulses have been employed for a pump-probe investigation of excited satellite states following  $4p^{-1}$  and  $4s^{-1}$  photoionization of Kr on the femtosecond time-scale.  $\text{Kr}^{+*}$  and  $\text{Kr}^{**}$  satellite states were populated by single high harmonics HH19 (29.6 eV), HH21 (32.8 eV), and HH23 (35.9 eV), and temporally delayed NIR pulses of variable intensities were used to probe the dynamics of these intermediate states via the creation of  $\text{Kr}^{2+}$  ground state ions. The delay-dependent NIR-XUV pump-probe studies in this work reveal a possibility to control the observed dynamics. We show, that by tuning the intensity of the NIR probing field in the range between  $0.3 \times 10^{13}$  to  $2.6 \times 10^{13} \text{ W cm}^{-2}$  it is possible (i) to control the ratio between sequential and non-sequential double ionization of Kr; (ii) to selectively probe quantum beating oscillations between  $\text{Kr}^{+*}$  satellite states excited by the XUV pulse; and (iii) to specifically probe short-lived ( $<150 \text{ fs}$ ) doubly excited ( $\text{Kr}^{**}$ ) decay channels. Our study demonstrates that the intensity of the NIR probing pulse is a critical experimental parameter for the multiple processes leading to doubly charged Kr ions through sequential and non-sequential pathways. As the NIR-probe intensity is increased, the sequential pathways through excited satellite states becomes more dominant in the contribution to the  $\text{Kr}^{2+}$  ion yield. In addition to the sequential and non-sequential contributions to the ion yield, NIR intensity-dependent oscillations, arising from quantum beating between neighboring satellite states, are observed. The amplitude of the quantum beat oscillations decreases with the NIR intensity for HH21 and increases for HH19. A possible explanation is the larger spread of final electronic states in the continuum at higher NIR intensities, as well as the potential coupling of the beating states to other satellite states with the NIR pulse.

Time-resolved XUV spectroscopy using HHG is a strong experimental technique for the study of ionization or de-excitation pathway. Our Kr ion charge-state spectroscopy investigation with HH19, HH21, and HH23 demonstrates the possibility to control contributions of certain ionization or de-excitation pathways by careful adjustment of the intensity of the NIR probing pulse. Combined with high-resolution photoelectron spectroscopy, this approach can contribute to further developments of time-resolved techniques using pulsed coherent XUV sources.














## Data availability statement

The data that support the findings of this study are available upon reasonable request from the authors.

## Acknowledgment

The authors acknowledge ELI Beamlines, Dolní Břežany, Czech republic, for the provided beamtime and thank facility staff for their assistance. The Institute of Physics of the Czech Academy of Sciences is acknowledged. The authors would also like to thank Rasmus Burlund Fink (Aarhus University, Denmark) for his support during the experiment, and Tim Oelze for his support during the data analysis. The authors are grateful to Zdenek Svoboda, the ELI Beamlines L1, control system teams, instrument group, and facility staff for their assistance and support during the project. This work was supported by the Projects Advanced research using high-intensity laser-produced photons and particles (ADONIS) (CZ.02.1.01/0.0/0.0/16\_019/0000789) and Structural dynamics of biomolecular systems (ELIBIO) (CZ.02.1.01/0.0/0.0/15\_003/ 0000447) (both from the European Regional Development Fund and the Ministry of Education, Youth and Sports). Part of this research was funded by the Extreme Light Infrastructure ERIC. L B L and M M are grateful for financial support from Danmarks Frie Forskningsfond (DFE) within the Project BE 6788/1-1:1, and from the Carlsberg Foundation. M M and C M acknowledge support within Projects MU 2347/12-1 and STI 125/22-2 of the Deutsche Forschungsgemeinschaft (DFG) in the frame of the Priority Programme 1840 QUTIF.

## ORCID iDs

Andreas H Roos  <https://orcid.org/0000-0001-8919-0979>  
Ziaul Hoque  <https://orcid.org/0000-0001-7869-6659>  
Eva Klimešová  <https://orcid.org/0000-0002-9569-7511>  
Ltaief Ben Ltaief  <https://orcid.org/0000-0002-6904-4648>  
Cristian Medina  <https://orcid.org/0000-0003-4202-1793>  
Matej Jurkovič  <https://orcid.org/0000-0002-4454-8268>  
Martin Albrecht  <https://orcid.org/0000-0002-0103-5614>  
Ondřej Finke  <https://orcid.org/0000-0002-3961-5446>  
Ondřej Hort  <https://orcid.org/0000-0002-1330-0825>  
Jaroslav Nejdil  <https://orcid.org/0000-0003-0864-8592>  
Marcel Mudrich  <https://orcid.org/0000-0003-4959-5220>  
Jakob Andreasson  <https://orcid.org/0000-0002-3202-2330>  
Maria Krikunova  <https://orcid.org/0000-0002-6152-1825>

## References

- [1] Schuurman M S and Blanchet V 2022 *Phys. Chem. Chem. Phys.* **24** 20012–24 Advance Article
- [2] Adachi S and Suzuki T 2018 *Appl. Sci.* **8** 1784
- [3] Calegari F, Sansone G, Stagira S, Vozzi C and Nisoli M 2016 *J. Phys. B: At. Mol. Opt. Phys.* **49** 062001
- [4] Young L *et al* 2018 *J. Phys. B: At. Mol. Opt. Phys.* **51** 032003
- [5] Feldhaus J, Krikunova M, Meyer M, Möller T, Moshhammer R, Rudenko A, Tschentscher T and Ullrich J 2013 *J. Phys. B: At. Mol. Opt. Phys.* **46** 164002
- [6] Squibb R J *et al* 2018 *Nat. Commun.* **9** 63
- [7] Ovcharenko Y *et al* 2014 *Phys. Rev. Lett.* **112** 073401
- [8] Oelze T *et al* 2017 *Sci Rep.* **7** 40736
- [9] Mudrich M and Steinkemeier F 2014 *Int. Rev. Phys. Chem.* **33** 301–39
- [10] Hütten K *et al* 2018 *Nat. Commun.* **9** 719
- [11] Krikunova M, Maltezopoulos T, Wessels P, Schlie M, Azima A, Wieland M and Drescher M 2011 *J. Chem. Phys.* **134** 024313
- [12] Uiberacker M *et al* 2007 *Nature* **446** 627–32
- [13] Krikunova M *et al* 2009 *New J. Phys.* **11** 13
- [14] Uphues T, Schultze M, Kling M F, Uiberacker M, Hendel S, Heinzmann U, Kabachnik N M and Drescher M 2008 *New J. Phys.* **10** 025009
- [15] Flögel M, Durá J, Schütte B, Ivanov M, Rouzée A and Vrakking M J J 2017 *Phys. Rev. A* **95** 021401
- [16] Johansson A *et al* 2003 *Eur. Phys. J. D* **22** 3–11
- [17] Bryan W A, Frassetto F, Froud C A, Turcu I C E, King R B, Calvert C R, Nemeth G R A J, Villorosi P, Poletto L and Springate E 2012 *New J. Phys.* **14** 013057
- [18] Verhoef A J, Mitrofanov A V, Nguyen X T, Krikunova M, Fritzsche S, Kabachnik N M, Drescher M and Baltuska A 2011 *New J. Phys.* **13** 113003
- [19] Klimesová E *et al* 2021 *Eur. Phys. J. Spec. Top.* **230** 4183–94
- [20] Hort O *et al* 2019 *Opt. Express* **27** 8871–83
- [21] Frassetto F, Fabris N, Miotti P and Poletto L 2017 *Photonics* **4** 14

- [22] Poletto L and Frassetto F 2018 *Appl. Sci.* **8** 5
- [23] Slattery A E, Wightman J P, MacDonald M A, Cvejanovic S and Reddish T J 2000 *J. Phys. B: At. Mol. Opt. Phys.* **33** 4833–48
- [24] Caló A, Atanassova S S, Sankari R, Kivimäki A, Aksela H and Aksela S 2006 *J. Phys. B: At. Mol. Opt. Phys.* **39** 4169
- [25] Yoshii H, Aoto T, Morioka Y and Hayaishi T 2007 *J. Phys. B: At. Mol. Opt. Phys.* **40** 2765
- [26] Alitalo S, Kivimäki A, Matila T, Vaarala K, Aksela H and Aksela S 2001 *J. Electron Spectrosc. Relat. Phenom.* **114–116** 141–6
- [27] Chuan Y and Madsen L B 2016 *Phys. Rev. A* **94** 053424
- [28] Jin F, Chen J, Yang Y, Yan Z-C and Wang B 2016 *J. Phys. B: At. Mol. Opt. Phys.* **49** 195602
- [29] Geiseler H, Rottke H, Steinmeyer G and Sandner W 2011 *Phys. Rev. A* **84** 033424
- [30] ten Wolde A, Noordam L D and Lagendijk A and 1988 van Linden van den Heuvell H B *Phys. Rev. Lett.* **61** 2099–101
- [31] Zamith S, Bouchene M A, Sokell E, Nicole C, Blanchet V and Girard B 2000 *Eur. Phys. J. D* **12** 255–61
- [32] Codling K and Madden R P 1972 *J. Res. Nat. Bur. Stand. A* **76A** 1–12
- [33] Lagutin B M, Sukhorukov V L, Petrov I D, Schmoranzler H, Ehresmann A and Schartner K-H 1994 *J. Phys. B: At. Mol. Phys.* **27** 5221–39